HHS Public Access

Author manuscript

Ann Thorac Surg. Author manuscript; available in PMC 2022 December 01.

Published in final edited form as:

Ann Thorac Surg. 2022 December ; 114(6): 2115–2123. doi:10.1016/j.athoracsur.2021.09.069.

3D Specimen Mapping Expedites Frozen Section Diagnosis of Nonpalpable Ground Glass Opacities

Gregory T. Kennedy, MD,

Feredun S. Azari, MD,

Elizabeth Bernstein, BA,

Charuhas Desphande, MD,

Azra Din, BA,

Isvita Marfatia, BA,

John C. Kucharczuk, MD,

Edward J. Delikatny, PhD,

Philip S. Low, PhD,

Sunil Singhal, MD

Department of Surgery, Perelman School of Medicine at the University of Pennsylvania, Philadelphia, Pennsylvania; Department of Pathology, Perelman School of Medicine at the University of Pennsylvania, Philadelphia, Pennsylvania; Department of Radiology, Perelman School of Medicine at the University of Pennsylvania, Philadelphia, Pennsylvania; and Department of Chemistry, Purdue University, West Lafayette, Indiana

Abstract

BACKGROUND—Pulmonary ground glass opacities (GGOs) are early-stage adenocarcinoma spectrum lesions that are not easily palpable. Challenges in localizing GGOs during intraoperative pathology can lead to imprecise diagnoses and additional time under anesthesia. To improve localization of GGOs during frozen section diagnosis, we evaluated a novel technique, 3-dimensional near-infrared specimen mapping (3D-NSM).

METHODS—Fifty-five patients with a cT1 GGO were enrolled and received a fluorescent tracer preoperatively. After resection, specimens were inspected to identify lesions. Palpable and nonpalpable nodules underwent 3D-NSM and the area of highest fluorescence was marked with a suture. Time for 3D-NSM, time for frozen section diagnosis, and number of tissue sections examined were recorded. To compare 3D-NSM with standard-of-care techniques, a control cohort of 20 subjects with identical inclusion criteria were enrolled. Specimens did not undergo 3D-NSM and were sent directly to pathology.

RESULTS—3D-NSM localized 54 of 55 lesions with 1 false negative. All 41 palpable lesions were identified by 3D-NSM. Thirteen (92.8%) of 14 nonpalpable lesions were located by 3D-NSM. Time to diagnosis for the 3D-NSM cohort was 23.5 minutes, compared with 26.0 minutes

Address correspondence to Dr Singhal, University of Pennsylvania Perelman School of Medicine, 3400 Spruce St, 6 White Bldg, Philadelphia, PA 19104; sunil.singhal@pennmedicine.upenn.edu.

Dr Low is a shareholder in On Target Laboratories. There are no conflicts of interest for any other author.

in the control cohort ($P = .04$). 3D-NSM did not affect time to diagnosis of palpable lesions (23.2 minutes vs 21.4 minutes; $P = .10$). 3D-NSM significantly reduced time to diagnosis for nonpalpable lesions (23.3 minutes vs 34.4 minutes; $P < .0001$). 3D-NSM also reduced the number of tissue sections analyzed in nonpalpable lesions (4.50 vs 11.00; $P < .0001$).

CONCLUSIONS—3D-NSM accurately localizes GGOs and expedites intraoperative diagnosis by reducing the number of tissue sections analyzed for nonpalpable GGOs.

Lung cancer screening by computed tomography detects thousands of suspicious pulmonary nodules annually.[1] A significant portion of these nodules are ground glass opacities (GGOs), ill-defined lesions marked by subtle parenchymal changes that often require resection for diagnosis and treatment.[2,3] Localization of GGOs is a formidable challenge intraoperatively for the surgeon and postoperatively for the pathologist, given the soft architecture of GGOs that complicates conventional visual and tactile localization. As a potential solution, our group and others have explored the use of intraoperative molecular imaging (IMI)–a technique that relies on systemic delivery of targeted fluorescent contrast agents that accumulate in lung nodules and can be detected using wavelength-specific camera systems.[4–10] However, the clinical challenge of localizing the nodule after resection and during pathologic analysis remains largely unaddressed.

Frozen section pathology during surgery for GGOs is critically important.[11] Suspicious lesions are removed by wedge resection, and intraoperative diagnosis frequently dictates the extent of resection. Specifically, the invasiveness of the lesion can direct the surgeon toward a limited wedge resection or a more extensive resection such as a segmentectomy or lobectomy.[12] Despite the importance of frozen section in decision making, it is an imperfect tool, with limitations in speed, diagnostic accuracy, and an inability to examine the entire resected specimen.[13] Challenges in sampling error are exacerbated in cases of small, visually occult, and difficult-to-palpate lesions. Additionally, nonpalpable lesions often require repeated sectioning for diagnosis, a resource-intensive process that prolongs time under anesthesia, increases morbidity for patients, and adds to health care costs.[11]

To improve the utility of frozen section pathology in patients undergoing IMI, we propose a novel technology–3-dimensional near-infrared specimen mapping (3D-NSM)–to assist the pathologist and provide realtime evaluation of an entire resected specimen. 3D-NSM can be used to precisely identify the target nodule and the most suspicious area of the nodule that should be analyzed by the pathologist. 3D-NSM utilizes 2 technologies. First, it is an extension of IMI using targeted fluorescent contrast agents.[14] Second, it utilizes a back table intraoperative imaging system that can spatially map the presence of tumor cells in a specimen.[15]

Here, we present the results of a single-center, nonrandomized pilot study of 3D-NSM (NCT02602119) for back table assessment of lung specimens. The objectives of the study were to (1) determine whether 3D-NSM accurately localizes GGOs once the specimen is removed, and (2) compare the time to diagnosis of traditional frozen section alone to 3D-NSM–guided pathology.

PATIENTS AND METHODS

STUDY DESIGN.

This study was approved by the University of Pennsylvania's Institutional Review Board. Fifty-five subjects with a small (T1) lung lesion suspicious for malignancy and with radiographic features suggestive of a difficult-to-palpate lesion (GGO with or without solid component) were enrolled between May 2016 and June 2020. Exclusion criteria included people under the age of 18 years, people unable to give informed consent, non–English-speaking people, and patients with prior chest surgery. All subjects gave written informed consent and were scheduled for minimally invasive wedge resection.

Participants received OTL38 (intravenous, 0.025 mg/kg) 6 to 24 hours before resection. The majority of patients received the tracer 24 hours before surgery, but there were a number of enrolled patients from remote locations that could not logistically arrange travel and lodging the night before surgery and were thus infused on the morning of surgery. All lesions were wedge resected using standard IMI techniques as described previously.[5] Briefly, a thoracoscope (VisionSense, New York, NY) capable of white-light and near-infrared (NIR) imaging was used to localize lesions. First, white-light thoracoscopy and thoracoscopic palpation were utilized to identify known lesions. Next, a $\lambda_{excitation}$ laser of 785 nm and $\lambda_{emission}$ bandpass filter of 800 to 835 nm were used to capture signal from the fluorescent probe that had localized to the lesion of interest.

After resection, the specimens were visually inspected and palpated to identify the lesion of interest on the back table. Palpable lesions were marked with a silk suture and confirmed using the 3D-NSM device. Nonpalpable lesions were imaged using the 3D-NSM device, and the resultant images were used to mark the area of highest fluorescence with a silk suture. The specimens were labeled "stitch marks nodule" and then hand-carried to the frozen section pathology analysis. Time for 3D-NSM and time for frozen section diagnosis were recorded prospectively, as was the number of tissue sections examined for each specimen. Specifically, the time to frozen section diagnosis was defined as the time when the specimen was removed from the operative field until the time that the frozen section diagnosis was called to the operating room. The time to 3D-NSM was defined as the time when the specimen was removed from the operative field until the 3D-NSM images were acquired.

To compare time to diagnosis with and without 3D-NSM, a control cohort of 20 subjects with identical inclusion criteria were enrolled. These patients were not infused with the study drug, and specimens were hand-carried directly to pathology after resection. Lesion palpability and time to frozen section diagnosis were recorded.

STUDY DRUG.

OTL38 ($C_{61}H_{63}N_9Na_4O_{17}S_4$, molecular weight: 1414.42 g/mol) is a folate analog conjugated to the NIR dye, S0456. OTL38 is characterized by excitation wavelength of 774 to 776 nm and emission wavelength of 794 to 796 nm. OTL38 targets the folate receptor (FR), which is expressed 90% of pulmonary adenocarcinomas and 70% of squamous cell carcinomas.[16,17] This drug was provided by On Target Laboratories (West Lafayette, IN). The safety and efficacy of OTL38 has been previously demonstrated.[5,6]

DEVICE FOR 3D-NSM.

The 3D-NSM system (ELVIS; LI-COR Biosciences, Lincoln, NE) is an experimental device that consists of a light-free space for closed-field fluorescence imaging (Figure 1). Specimens are placed on a moving stage that allows image capture from multiple viewing angles along 2 rotational axes. The controlled light sources include laser diodes at 785 nm and visible white-light light-emitting diodes. Fluorescence images were collected through an 800-nm channel with center wavelength at 820 nm. These settings were chosen by the manufacturer and centered over the absorption and emission wavelengths of indocyanine green to be compatible with multiple existing NIR tracers. A control program (based on LabVIEW; National Instruments, Austin TX) ran the imaging process connected to a customized Image Studio software (LI-COR Biosciences) for imaging collection, storage, and analysis.

POST HOC IMAGE ANALYSIS.

Mean fluorescence intensity of the lesion (MFI_{lesion}) was obtained by analyzing NIR images with ImageJ (version 1.53e National Institutes of Health, Bethesda, MD; http://rsb.info.nih.gov/ij) and measuring the region of interest that correlated to the lesion. Background fluorescence was also obtained ($MFI_{background}$). A minimum of 1000 pixels were included in each measurement. Calculations were repeated in triplicate from varying angles, and signal-to-background fluorescence ratios (SBRs) were calculated. SBR assessments were averaged, and a mean SBR greater than 2.0 was considered fluorescent.

HISTOPATHOLOGIC AND FLUORESCENT MICROSCOPIC REVIEW OF SPECIMENS.

Specimens were formalin fixed and paraffin embedded. Sequential 5-μm sections were obtained and underwent comprehensive histopathologic and fluorescent analysis by a board-certified thoracic pathologist. Sections were stained using standard hematoxylin and eosin staining. Immunohistochemical staining for FRα was also performed. To understand OTL38 accumulation patterns at a microscopic level, an additional unstained 5-μm section was evaluated using an NIR microscopic scanner (Odyssey; LI-COR Biosciences) and an NIR microscope (Leica Microsystems, Buffalo Grove, IL). Areas of fluorescence were then correlated to both hematoxylin and eosin and anti-FRα immunohistochemical specimens.

STATISTICAL ANALYSIS.

Owing to the exploratory nature of this study, logistic regression was used to determine patient and histopathologic variables associated with lesion fluorescence. Comparisons were made using Stata release 14 (StataCorp, College Station, TX). A P value less than .05 was considered statistically significant.

RESULTS

PATIENT AND LESION CHARACTERISTICS.

The patients in the study cohort tended to be middle-aged (mean age 68.3 years) (Table 1), female (n = 30, 54.5%), and former smokers (33.7 mean pack years). All patients had a preoperative computed tomography scan and positron emission tomography scan that

suggested a GGO, and mean consolidation-to-tumor ratio of patients in the study was 0.52. Mean lesion size was 1.7 cm and mean depth was 0.5 cm from the pleural surface. Lesions were distributed throughout the anatomic lobes of the lung. After resection, the specimens were assessed by visual inspection and finger palpation by 2 surgeons on the back table. The majority of lesions were palpable on the back table (n = 41, 74.5%), although the remaining 14 lesions could not be clearly identified by visual inspection or manual palpation.

3D-NSM LOCALIZES PALPABLE AND NONPALPABLE PULMONARY LESIONS.

Bimanual back table palpation localized 41 of 55 nodules with 14 false negatives for an accuracy of 75%. After completing the standard-of-care back table assessment, 3D-NSM was performed on all specimens. All of the 41 palpable lesions were localized by 3D-NSM. Of the 14 nonpalpable lesions, 13 (93%) were able to be clearly identified by 3D-NSM. The lone lesion unable to be located by palpation or 3D-NSM was a small granuloma (0.8 cm in greatest dimension) deep to the pleural surface that required repeated sectioning for diagnosis by frozen section pathology. Figure 2 shows representative images of nonpalpable lesions that were localized by 3D-NSM. In total, 3D-NSM localized 54 of 55 lesions with 1 false negative in the study cohort for an accuracy of 98% (Figure 3A). Receiver-operating characteristic curve evaluation (Figure 3B) showed that the area under the curve obtained for lesion MFI was 0.977 (95% confidence interval, 0.954–0.999).

Both palpable and nonpalpable lesions were distinct from the background lung parenchyma with significantly greater MFI than surrounding tissue (Figure 3C). There were no statistically significant differences in MFI (mean MFI for palpable lesions = 95.7 AU, nonpalpable lesions = 98.0 AU) or SBR (mean SBR for palpable lesions = 4.40, nonpalpable lesions = 4.51) between nonpalpable and palpable lesions (Figure 3D). Malignant lesions displayed significantly greater fluorescence than benign lesions (Figure 3E). The mean SBR for adenocarcinomas was 4.55, for squamous cell carcinoma was 5.38, for small cell lung cancer was 5.20, and for other malignancy was 3.80. The mean SBR for benign lesions was 1.80.

LESION HISTOPATHOLOGY AND MICROSCOPIC FLUORESCENCE.

By the final histopathologic analysis, the majority of lesions were invasive adenocarcinomas (n = 36, 65.5%). The other lesions were adenocarcinomas in situ (n = 1, 1.8%), squamous cell carcinoma of the lung (n = 4, 7.3%), small cell lung cancer (n = 3, 5.5%), metastases from nonpulmonary cancers (n = 5, 9.1%), carcinoid tumors (n = 2, 3.6%), mesothelioma (n = 1, 1.8%), spindle cell carcinoma (n = 1, 1.8%) or benign lesions (n = 2, 3.6%). There were no significant differences in lesion diagnosis when comparing palpable with nonpalpable lesions.

To better understand the microscopic patterns of the macroscopically fluorescent nodules, all lesions were serially sectioned and stained with hematoxylin and eosin, as well as with immunohistochemistry staining for FRα. These sections were compared with adjacent sections that were imaged by an NIR fluorescence scanner and subsequently by an immunofluorescence microscope. In all fluorescent nodules, the microscopically

fluorescent areas correlated spatially with malignant cells expressing FRα (see Figure 4 for representative cases).

3D-NSM EXPEDITES TIME TO DIAGNOSIS OF GGOS.

To determine whether 3D-NSM affected the time to diagnosis of lesions, we prospectively recorded the time from specimen removal to the communication of frozen section diagnosis by pathologists. We compared time to diagnosis of patients in the study cohort with a control cohort of 20 patients that were not infused with OTL38 or imaged with 3D-NSM (Figure 4). Of the 20 control patients, 13 had lesions that were palpable on the back table and 7 patients had nonpalpable lesions.

For all patients, mean time to frozen section diagnosis was 24.2 (interquartile range, 21.0–26.0) minutes. Time to diagnosis for the 3D-NSM cohort was 23.5 minutes, compared with 26.0 minutes in the control cohort ($P = .04$). Among the control cohort, time to diagnosis was significantly longer for nonpalpable lesions as compared with palpable lesions (34.4 minutes vs 21.4 minutes; $P < .0001$).

For all patients in the experimental arm, mean time for 3D-NSM was 2.2 (interquartile range, 1.6–3.1) minutes. 3D-NSM did not affect time to diagnosis of palpable lesions (23.2 minutes vs 21.4 minutes; $P = .10$). However, lesion marking with 3D-NSM significantly reduced the time to diagnosis for nonpalpable lesions (23.3 minutes vs 34.4 minutes; $P < .0001$). Most notably, there was no significant difference between time to diagnosis for palpable and nonpalpable lesions when guided by 3D-NSM ($P = .31$).

3D-NSM REDUCES NUMBER OF SPECIMEN SECTIONS IN NONPALPABLE LESIONS.

To explain why 3D-NSM reduces time to diagnosis in nonpalpable lesions, we first evaluated whether there was a correlation between number of tissue sections analyzed and time to diagnosis among all lesions. We found that there was a strong positive correlation between the number of tissue sections performed and the time to frozen section diagnosis (coefficient of determination $R^2 = 0.71$) (Figure 5B). The average number of sections for palpable and nonpalpable lesions was 3.31 and 6.67, respectively. Imaging by 3D-NSM did not affect the number of sections analyzed for palpable lesions (3.34 for 3D-NSM-guided pathology vs 3.23 in the control cohort; $P = .61$). However, 3D-NSM significantly reduced the number of sections analyzed in nonpalpable lesions when compared with the control cohort (4.50 vs 11.00; $P < .0001$).

We observed 2 possible explanations for these findings. First, we observed that the presence of the silk suture directed more rapid decision making by the pathologist, allowing them to precisely section tissue in the region of interest. Second, if the pathologist could not confidently make a diagnosis when no stitch was present, additional sections or deeper cuts were performed.

COMMENT

Reliable rapid localization of pulmonary GGOs is a formidable challenge. The scope of this problem is increasing with improvements in imaging technology and increasing use

of computed tomography screening for cancer, which detects a vast number of small lesions that are suspicious for cancer and require resection for diagnosis.[3] The exact cutoffs for when these GGOs should be removed is evolving and the topic of other studies.[18] Growing evidence suggests that sublobar pulmonary resection with appropriate margins for these early lesions is likely equivalent to lobectomy in rates of recurrence and survival, underscoring the importance of GGO localization.[19] This clinical trial validates a novel technique, 3D-NSM, for the localization of GGOs and demonstrates its efficacy in expediting time to frozen section diagnosis.

3D-NSM is an innovation that stems from 2 emerging technologies that have gained prominence within surgical oncology in recent years. The first is IMI, a technology that utilizes systemic delivery of tumor-targeted tracers that selectively labels malignant cells. The second is the back table imaging device in which 3D-NSM is performed. This calibrated camera system consists of an ambient, light-free space for closed-field fluorescence imaging, with a moving stage allowing image capture from a variety of viewing angles along 2 rotational axes. The fluorescent images are then configured by image analysis software to produce a 3D reconstruction of the specimen with the precise location of the fluorescent lesion in space. Previous work by our group and others have demonstrated the utility of IMI in the resection of solid tumors, but this study finds particular value for this technology in the management of difficult-to-palpate nodules.[15,20] The clinical utility of IMI and 3D-NSM may be greatest in nonpalpable, visually occult lesions as an adjunct to the traditional surgical and pathologic methods of lesion identification.

Current intraoperative diagnosis and margin assessment relies on frozen section pathology, a critical tool with important limitations. First, only a small fraction of specimens can be sampled with identification of suspicious areas based on visual inspection and palpation. The diagnostic specificity of frozen section is limited by time constraints and lack of definitive tissue staining.[13] Finally, the process is time- and resource-intensive.[11] These challenges are exacerbated in the case of small, nonpalpable, and visually occult tumors, which are often marked by only subtle parenchymal distortions and can be difficult to distinguish from surrounding parenchyma.[13]

As demonstrated by this trial, 3D-NSM allows for precise localization of these nonpalpable lesions. In doing so, pathologists are able to selectively section the region of interest that has fluoresced on 3D-NSM, rather than repeatedly section the specimen in a nonselective manner. Reduction in the number of tissue sections needed for diagnosis will have important benefits in the cases of small lesions, allowing more tissue to be preserved for advanced immunohistologic staining and genetic analysis.

We further anticipate that this technology will provide important benefits in the streamlining of care and reduction in resource utilization in an era of cost containment. At tertiary referral centers, specialized pathologists are often consulted in cases of diagnostic uncertainty or difficulty in lesion identification during frozen section diagnosis. 3D-NSM may reduce the need for specialist consultation and also give pathologists a higher level of confidence that they have localized the lesion of interest. This focused approach reduces the number of sections needed for diagnosis, and speeds the overall time to communication of the

diagnosis to the surgical team. Ultimately, we anticipate that this technology will have important clinical benefits for patients who will undergo targeted, sublobar resections where appropriate, and be spared the morbidity of additional time under anesthesia for frozen section diagnosis.

The precise cost effectiveness of the 3D-NSM approach is difficult to evaluate in the present pilot study and was not the primary outcome. However, we anticipate that there may be net cost savings associated with the 3D-NSM approach due to reductions in operative time. A recently published analysis of over 300 California hospitals estimated that the cost of 1 minute of operative time was $37.37 in the inpatient setting,[21] and that the costs of operative time have increased at a rate higher than the consumer price index. Extrapolating from these findings, the cost savings associated with a reduction in operative time of 11.1 minutes–as seen in nonpalpable GGOs in our study cohort–would translate to a reduced operative cost of $400 per patient. The exact startup costs associated with purchasing the 3D-NSM device and establishing a workflow for OTL38 infusion are difficult to estimate at this time, given that neither technology is commercially available. We anticipate that economies of scale as the technology is adopted clinically will help drive down these costs and contribute to the overall cost effectiveness of the technology. As part of the ongoing evaluation of the potential clinical benefits of the 3D-NSM technology, a more precise cost effectiveness will also need to be elucidated.

An important consideration in this study is that the patients are already scheduled to undergo in vivo IMI. This technology has been the focus of other reports.[6] Despite the efficacy of IMI with regard to lesion localization in vivo, GGOs can still be quite challenging to find on the back table and during pathological analysis. This study shows clear benefits of 3D-NSM technology for this particular aspect of the operative workflow. Other approaches to back table lesion localization have been tried, including computed tomography scanning of specimens and rapid polymerase chain reaction testing, but these technologies have been cumbersome, impractical, and time-consumptive.[22,23]

We acknowledge several limitations in this trial. This exploratory study was not randomized and consisted of a small number of patients at a single institution. Additional randomized studies at multiple institutions are needed to confirm efficacy and justify further clinical development. This trial uses a probe that specifically targets malignant cells that overexpress FRα and is thus not useful in tumors without this receptor expression profile. We anticipate that the clinical utility of 3D-NSM will expand as targeted tracers are developed for other malignancies. Despite these limitations, this trial demonstrates the potential of this technology in managing nonpalpable pulmonary tumors.

Acknowledgments

Dr Kennedy was supported by the American Philosophical Society and the National Institutes of Health (grant F32CA254210-01). Dr Azari was supported by The Society for Thoracic Surgeons. Dr. Singhal was supported by the National Institutes of Health (grant R01CA193556) and the State of Pennsylvania Health Research Formula Fund.

REFERENCES

1. Krist AH, Davidson KW, Mangione CM, et al. Screening for lung cancer: US preventive services task force recommendation statement. JAMA. 2021;325(10):962–970. [PubMed: 33687470]
2. Azari F, Kennedy G, Singhal S. Intraoperative detection and assessment of lung nodules. Surg Oncol Clin N Am. 2020;29(4):525–541. [PubMed: 32883456]
3. Pedersen JH, Saghir Z, Wille MMW, Thomsen LH, Skov BG, Ashraf H. Ground-glass opacity lung nodules in the era of lung cancer CT screening: radiology, pathology, and clinical management. Oncology (Williston Park). 2016;30(3):266–274. [PubMed: 26984222]
4. Kennedy GT, Azari FS, Bernstein E, et al. Targeted intraoperative molecular imaging for localizing nonpalpable tumors and quantifying resection margin distances. JAMA Surg. 2021;156(11):1043–1050. 10.1001/jamasurg.2021.3757 [PubMed: 34431971]
5. Predina JD, Newton AD, Keating J, et al. A phase I clinical trial of targeted intraoperative molecular imaging for pulmonary adenocarcinomas. Ann Thorac Surg. 2018;105(3):901–908. [PubMed: 29397932]
6. Gangadharan S, Sarkaria I, Rice D, et al. Multi-institutional phase 2 clinical trial of intraoperative molecular imaging of lung cancer. Ann Thorac Surg. 2021;112(4):1150–1159. 10.1016/j.athoracsur.2020.09.037 [PubMed: 33221195]
7. Newton AD, Kennedy GT, Predina JD, Low PS, Singhal S. Intraoperative molecular imaging to identify lung adenocarcinomas. J Thorac Dis. 2016;8(Suppl 9):S697–S704. [PubMed: 28066672]
8. Kennedy GT, Okusanya OT, Keating JJ, et al. The optical biopsy: A novel technique for rapid intraoperative diagnosis of primary pulmonary adenocarcinomas. Ann Surg. 2015;262(4):602–609. [PubMed: 26366539]
9. Predina JD, Newton A, Kennedy G, Lee MK, Singhal S. Near-infrared intraoperative imaging can successfully identify malignant pleural mesothelioma after neoadjuvant chemotherapy. Mol Imaging. 2017;16:1–3.
10. Kennedy GT, Newton A, Predina J, Singhal S. Intraoperative near-infrared imaging of mesothelioma. Transl Lung Cancer Res. 2017;6(3): 279–284. [PubMed: 28713673]
11. Sienko A, Allen TC, Zander DS, Cagle PT. Frozen section of lung specimens. Arch Pathol Lab Med. 2005;129(12):1602–1609. [PubMed: 16329732]
12. Liu S, Wang R, Zhang Y, et al. Precise diagnosis of intraoperative frozen section is an effective method to guide resection strategy for peripheral small-sized lung adenocarcinoma. J Clin Oncol. 2016;34(4):307–313. [PubMed: 26598742]
13. Walts AE, Marchevsky AM. Root cause analysis of problems in the frozen section diagnosis of in situ, minimally invasive, and invasive adenocarcinoma of the lung. Arch Pathol Lab Med. 2012;136(12):1515–1521. [PubMed: 23194044]
14. Tipirneni KE, Warram JM, Moore LS, et al. Oncologic procedures amenable to fluorescence-guided surgery. Ann Surg. 2017;266(1):36–47. [PubMed: 28045715]
15. Teraphongphom N, Kong CS, Warram JM, Rosenthal EL. Specimen mapping in head and neck cancer using fluorescence imaging. Laryngoscope Investig Otolaryngol. 2017;2(6):447–452.
16. Low PS, Henne WA, Doorneweerd DD. Discovery and development of folic-acid-based receptor targeting for imaging and therapy of cancer and inflammatory diseases. Acc Chem Res. 2008;41(1):120–129. [PubMed: 17655275]
17. Parker N, Turk MJ, Westrick E, Lewis JD, Low PS, Leamon CP. Folate receptor expression in carcinomas and normal tissues determined by a quantitative radioligand binding assay. Anal Biochem. 2005;338(2): 284–293. [PubMed: 15745749]
18. Sagawa M, Oizumi H, Suzuki H, et al. A prospective 5-year follow-up study after limited resection for lung cancer with ground-glass opacity. Eur J Cardiothorac Surg. 2018;53(4):849–856. [PubMed: 29236995]
19. Altorki NK, Yip R, Hanaoka T, et al. Sublobar resection is equivalent to lobectomy for clinical stage 1A lung cancer in solid nodules. J Thorac Cardiovasc Surg. 2014;147(2):754–764. [PubMed: 24280722]

20. van Keulen S, van den Berg Nynke S, Nishio N, et al. Rapid, noninvasive fluorescence margin assessment: optical specimen mapping in oral squamous cell carcinoma. Oral Oncol. 2019;88:58–65. [PubMed: 30616798]

21. Childers CP, Maggard-Gibbons M. Understanding costs of care in the operating room. JAMA Surg. 2018;153(4):e176233. [PubMed: 29490366]

22. Troschel FM, Gottumukkala RV, DiCorpo D, et al. Feasibility of perioperative micro-computed tomography of human lung cancer specimens: a pilot study. Arch Pathol Lab Med. 2019;143(3):319–325. [PubMed: 30457896]

23. Raja S, Ching J, Xi L, et al. Technology for automated, rapid, and quantitative PCR or reverse transcription-PCR clinical testing. Clin Chem. 2005;51(5):882–890. [PubMed: 15746302]

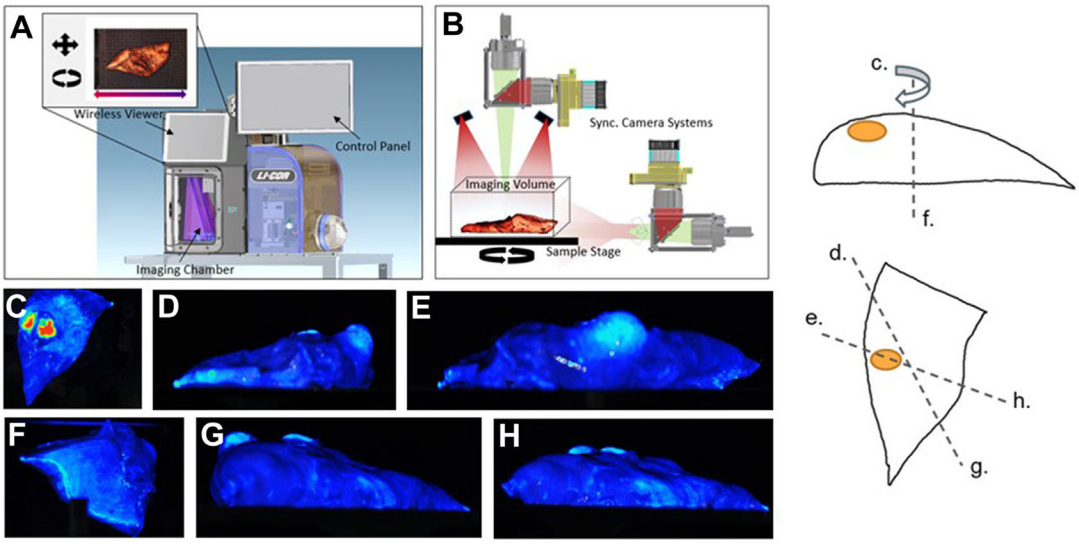

FIGURE 1.

Three-dimensional near-infrared specimen mapping device. (A, B) The device consists of a light-free space for closed field fluorescence imaging. (C-H) Specimens are placed on a moving stage that allows image capture from a variety of viewing angles along 2 rotational axes.

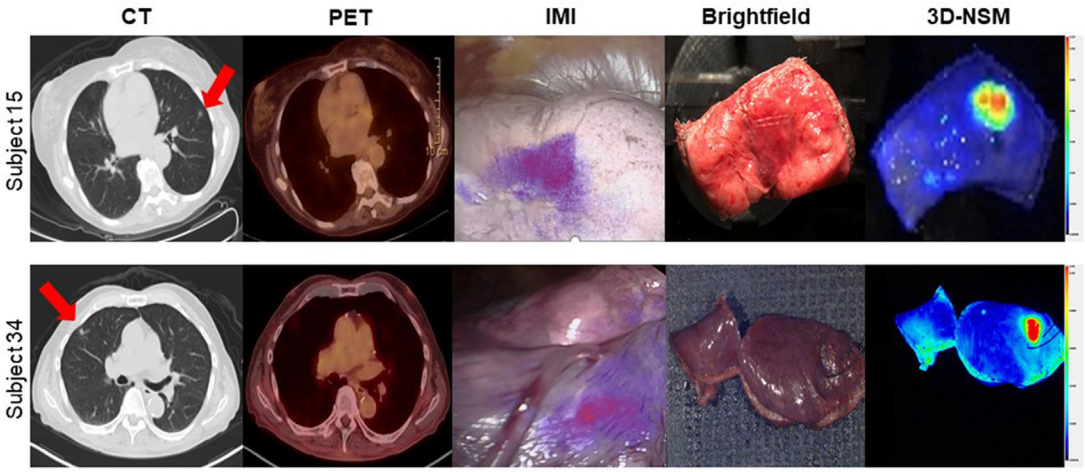

FIGURE 2.

Three-dimensional near-infrared specimen mapping (3D-NSM) localizes nonpalpable pulmonary lesions. This figure shows representative images from 2 patients with nonpalpable pulmonary lesions enrolled in the study. Preoperative computed tomography (CT) and positron emission tomography (PET) images are shown on the left with red arrows denoting lesions. The center panel shows brightfield images in which lesions cannot clearly be identified by visual inspection and palpation but are highly fluorescent on 3D-NSM.

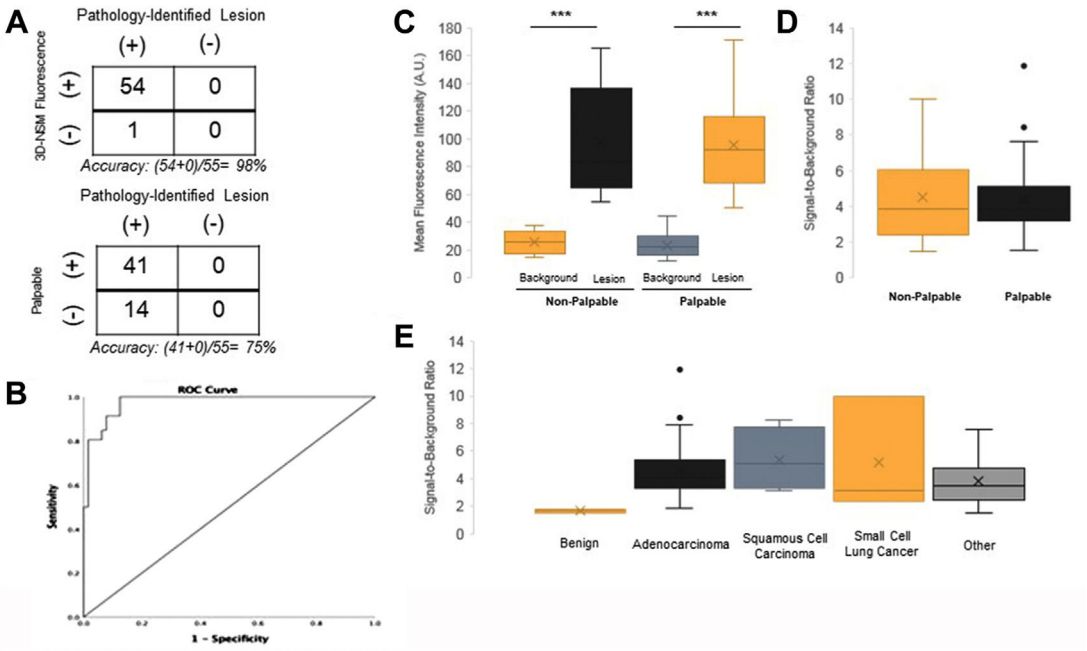

FIGURE 3.

Three-dimensional near-infrared specimen mapping (3D-NSM) fluorescence locates pulmonary ground glass opacities (GGOs). (A) Two by two tables comparing the accuracy of 3D-NSM in locating GGOs with the accuracy of finger palpation in locating GGOs. 3D-NSM had 1 false negative as compared with 14 false negatives by palpation. (B) Receiver-operating characteristic (ROC) curve evaluation for lesion mean fluorescence intensity. (C) denotes the mean fluorescence intensity of lesions and the background tissue when stratified by palpability. The mean fluorescence intensities of both palpable and nonpalpable GGOs were significantly higher than background tissue. (D) The signal-to-background ratios of nonpalpable lesions as compared with palpable lesions. (E) The signal-to-background ratios of all lesions when stratified by histopathological diagnosis. ***$P < .0001$.

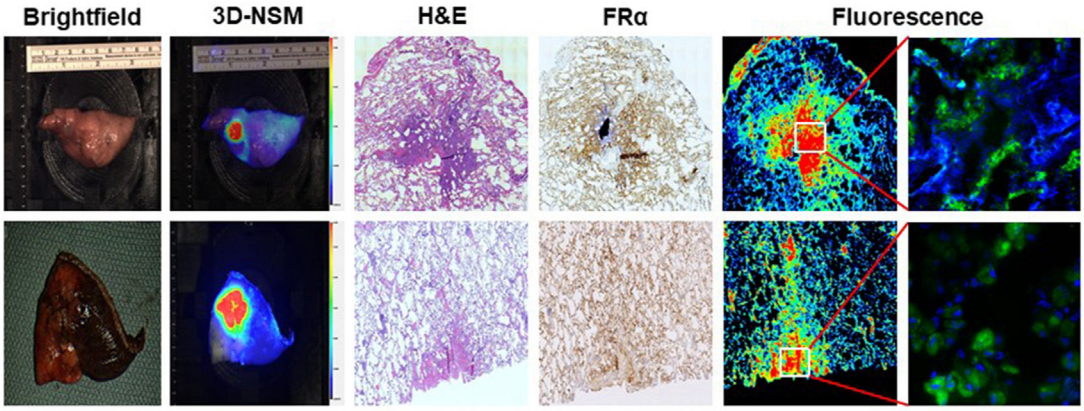

FIGURE 4.

Correlation of macroscopic fluorescence with folate receptor alpha (FRα) expression in lung lesions. This figure shows representative images of patients in the study that underwent 3-dimensional near-infrared specimen mapping (3D-NSM). The leftmost 2 columns show macroscopic brightfield and 3D-NSM images, respectively. The center column shows microscopic evaluation of the specimens after hematoxylin and eosin staining. The rightmost 3 columns show immunohistochemistry analysis for FRα expression and fluorescence microscopy, showing clear correlation between the areas of highest FRα expression and brightest fluorescence. (H&E, hematoxylin and eosin.)

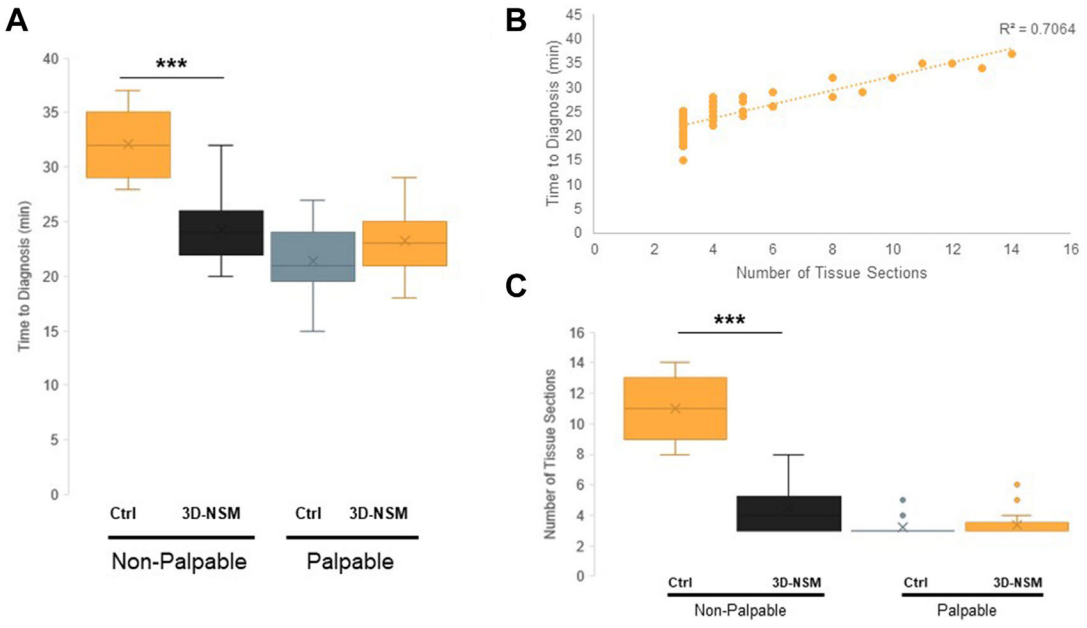

FIGURE 5.

Three-dimensional near-infrared specimen mapping (3D-NSM) expedites time to frozen section diagnosis of nonpalpable lesions. (A) Time to frozen section diagnosis, comparing 3D-NSM-guided pathology with the control cohort undergoing standard frozen section. When stratified by lesion palpability, 3D-NSM significantly reduced time to diagnosis for nonpalpable lesions but did not affect time to diagnosis of palpable lesions. (B) The correlation of number of tissue sections performed with the time to frozen section diagnosis, showing a strong positive correlation with $R^2 = 0.7064$. (C) The number of tissue sections cut per specimen, comparing 3D-NSM–guided pathology with the control cohort undergoing standard frozen section. When stratified by lesion palpability, 3D-NSM significantly reduced the number of specimen sections taken, suggesting that this is the mechanism by which 3D-NSM expedites frozen section diagnosis of nonpalpable lesions. ***$P < .0001$. (Ctrl, control.)

TABLE 1

Patient and Lesion Characteristics

Characteristic	Value
Sex	
Male	25 (45.5)
Female	30 (54.5)
Age, y	68.3 ± 9.4
Pack-years	33.7 ± 32.9
Hours between infusion and imaging	14.6 ± 9.5
Lesion characteristics	
PET SUV	3.4 ± 2.6
Lesion size, cm	1.7 ± 0.8
Lesion depth on imaging, cm	0.5 ± 0.7
Consolidation-to-tumor ratio	0.52 ± 0.08
Palpable ex vivo	41 (74.5)
Location	
RUL	16 (29.0)
RML	3 (5.4)
RLL	14 (25.5)
LUL	14 (25.5)
LLL	8 (14.5)
Final pathology	
Benign	2 (3.6)
Non-small cell carcinoma	41 (74.5)
Adenocarcinoma	36 (65.5)
Adenocarcinoma in situ	1 (1.8)
Squamous cell carcinoma	4 (7.3)
Small cell carcinoma	3 (5.5)
Metastasis	5 (9.1)
Other	4 (7.3)
Tumor differentiation	
Well	6 (10.9)
Moderate	24 (43.6)
Poor	14 (25.5)
Not reported	11 (20.0)
Operation performed	
Wedge resection	11 (20.0)
Segmentectomy	8 (14.5)
Lobectomy	36 (65.5)

Values are n (%) or mean ± SD. LLL, left lower lobe; LUL, left upper lobe; PET, positron emission tomography; RLL, right lower lobe; RML, right middle lobe; RUL, right upper lobe; SUV, standardized uptake value.